CO2 Hydrogenation over Oxide-Supported PtCo Catalysts: The Role of the Oxide Support in Determining the Product Selectivity

Shyam Kattel, Weiting Yu, Xiaofang Yang, Binhang Yan, Yanqiang Huang, Weiming Wan, Ping Liu, and Jingguang G. Chen

Chemistry Department

Brookhaven National Laboratory

DISCLAIMER

CO₂ Hydrogenation on Oxide-supported PtCo Catalysts: Fine-tuning Selectivity using Oxide Supports

Shyam Kattel,[a],# Weiting Yu,[b],# Xiaofang Yang,[a] Binhang Yan,[a] Yanqiang Huang,[c] Weiming Wan,[b] Ping Liu,*[a] and Jingguang G. Chen*[a,b]

Abstract: Fine-tuning of catalytic activity and selectivity has been one of the grand challenges in catalysis. Here, we report that by simply varying oxide supports the selectivity of metal/oxide catalysts can be finely tuned. Using CO_2 hydrogenation over PtCo bimetallic catalysts supported on different reducible oxides (CeO_2, ZrO_2, and TiO_2) as a case study, our combined experiment-theory study indicates that the variation from TiO_2 to CeO_2 or ZrO_2 introduces a selective strengthening in bindings of the C,O-bound and O-bound species at the PtCo-oxide interface, leading to a different product selectivity. These results reveal mechanistic insights in fine-tuning the catalytic performance of metal-oxide catalysts.

Catalyst performances strongly depend on the binding properties. Following the Sabatier principle,[1] a good catalyst should bind the reaction intermediates strongly enough to activate the reactants, and weakly enough to desorb the products. Various approaches have been applied to optimize the structure of a catalyst and to tune the binding properties and therefore catalytic activities. Typically, a linear scaling response is observed for the binding energies of various adsorbates upon, for instance, varying the local structures of a catalyst or the composition to form mono- or bi-metallic alloys across the Periodic Table.[2] As a result, the catalytic activity toward a reaction can be enhanced via accelerating the activity-limiting steps along the reaction pathway;[3] however it makes the control of product selectivity relatively more difficult, which often requires the non-linear tuning in binding energies of different adsorbate species.

Here, we report one of the possibilities to move away from the linear scaling by taking advantages of the strong metal-oxide interaction to selectively modify the binding energies of adsorbates. The special synergy between metals and oxides can introduce large electronic perturbations in the metals, [4] provide heterogeneous sites[3d, 5] or induce variation in the structure or phase on the supported metal particles,[6] which directly affects the bonding properties and correspondingly the catalytic performances. Carbon dioxide (CO_2) hydrogenation on PtCo bimetallic catalysts supported on different reducible oxides (CeO_2, ZrO_2, and TiO_2) was taken as a case study. By using different oxide supports, the binding of metal-oxide interface to various reaction intermediates varies; however the response is very different depending on the species. Such non-linear response enables the significant tuning in the selectivity of metal-oxide catalysts; in contrast much smaller effect is observed for the overall activity. The combination of Ambient Pressure X-ray Photoelectron Spectroscopy (AP-XPS) and Density Functional Theory (DFT) calculations for model catalysts and Transmission Electron Microscopy (TEM), Fourier Transform Infrared (FTIR) spectroscopy, Diffuse Reflectance Infrared Fourier Transform Spectroscopy (DRIFTS), and Extended X-ray Absorption Fine Structure (EXAFS) for the

corresponding powder catalysts allows us to reveal mechanistic insights in fine-tuning the catalytic performance of metal-oxide catalysts.

The catalytic conversion of CO_2 for the production of methane (CH_4)[6c, 7], methanol (CH_3OH)[3d, 8], and carbon monoxide (CO)[6c, 9] has gained tremendous interest in recent years. CH_4 from CO_2 conversion is not profitable considering the high shale gas reserve and its low volumetric energy density. The CH_3OH synthesis is well studied, but the current market demand for CH_3OH would only reduce 0.1% of the global CO_2 emission if all CH_3OH is produced using CO_2.[10] Thus, one of the most desirable routes for CO_2 conversion is to produce CO, the feedstock for the Fischer-Tropsch process to produce chemicals and fuels. Achieving a high selectivity to the desired CO product rather than CH_4 and CH_3OH is critical, yet challenging for practical applications.
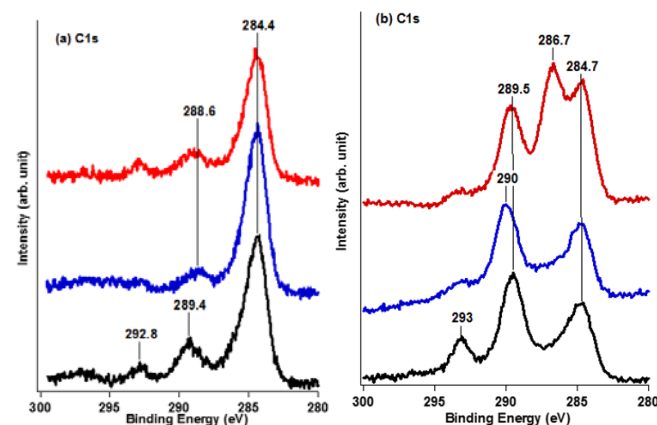

Figure 1. AP-XPS of C1s for (a) PtCo/TiO_2 and (b) PtCo/CeO_2 after the exposure of 100 mTorr CO_2 and 600 mTorr H_2 (black: 30 °C, blue: heating to 250 °C, red: heating to 250 °C and then cooling down to 30 °C).

Metal-based catalysts on oxide supports are active for the catalytic conversion of CO_2. Cu-based catalysts have been found to be active to covert CO_2 and hydrogen to CH_3OH,[8a, 11] while Pt-, Au- and Ag-based catalysts promote CO_2 conversion to CO.[12] In the present study, we demonstrate an example of fine-tuning the selectivity of PtCo catalysts by using oxides, where PtCo/TiO_2 catalyst is effective in converting CO_2 and H_2 to CO and PtCo/CeO_2 and PtCo/ZrO_2 catalysts are found to be selective to CH_4. Because PtCo/CeO_2 and PtCo/ZrO_2 show similar behavior (see SI), either PtCo/CeO_2 or PtCo/ZrO_2 is used as a representative to compare with PtCo/TiO_2.

Because CO_2 does not adsorb strongly on single crystal surfaces under ultrahigh vacuum conditions, AP-XPS measurements on PtCo/TiO_2(110) and PtCo/CeO_2(110) model surfaces were performed to identify possible reaction intermediates for CO_2 reduction by H_2. The C1s peaks of surface species at 292.8 eV for PtCo/TiO_2(110) (Figure 1a) and 293 eV for PtCo/CeO_2(110) (Figure 1b) denote gas phase CO_2. The features at 289.4 eV in Figure 1a and 289.5 eV in Figure 1b are attributed to the formation of carbonate (*CO_3) or formate (*HCOO)/carboxyl (*HOCO) species on both surfaces. These surface intermediates have been identified by AP-XPS on the CeO_x/Cu(111) surface after exposure to CO_2 at ambient pressures.[3d, 13] The peaks around 284.4 eV in Figure 1a and 284.7 eV in Figure 1b indicate the presence of carbon on both surfaces. Upon heating to 250 °C and cooling down to room temperature, there is a peak around 286.7 eV for PtCo/CeO_2(110) but not for PtCo/TiO_2(110). This peak

[a] Dr. S. Kattel, Dr. X. Yang, Dr. B. Yan, Dr. P. Liu, Dr. J. G. Chen
     Chemistry Department, Brookhaven National Laboratory
     2 Center St., Upton, NY 11973 (USA)
     E-mail: pingliu3@bnl.gov
[b] Dr. W. Yu, W. Wan, Prof. Dr. J. G. Chen
     Department of Chemical Engineering, Columbia University
     1500 W. 120th St., New York, NY 10027 (USA)
     E-mail: jgchen@columbia.edu
[c] Y. Huang
     Dalian Institute of Chemical Physics, Chinese Academy of Science
     Dalian, China, 116023
[#] Dr. S. Kattel and Dr. W. Yu contributed equally to this work.
     Supporting information for this article is given via a link at the end of the document.

corresponds to the formation of methoxy (*CH$_3$O), suggesting that CO$_2$ hydrogenation may follow different reaction pathways on the PtCo/TiO$_2$(110) and PtCo/CeO$_2$(110) surfaces, which will be confirmed using supported powder catalysts.

Table 1. Particle size, coordination number (CN), CO chemisorption, steady-state CO$_2$ conversion, turnover frequency (TOF) and CO/CH$_4$ ratio on PtCo/TiO$_2$, PtCo/CeO$_2$ and PtCo/ZrO$_2$ catalysts.

Catalysts	PtCo/TiO$_2$	PtCo/CeO$_2$	PtCo/ZrO$_2$
Particle size (nm)	2.3±0.5	2.7±1.0	2.3±0.7
CN (Pt-Pt)	4.2 ± 0.6	5.1 ± 1.3	4.3 ± 2.1
CN (Pt-Co)	1.7 ± 0.5	2.7 ± 0.6	2.3 ± 1.6
CO chemisorption (μmol/g)	18.7	36.4	39.4
CO$_2$ conversion (%)	8.2	9.1	7.8
TOF (min^{-1})	35.3	20.1	16.0
CO/CH$_4$ ratio	85	12	8.5

The TEM results in Tables 1 and Figure S1 show that the size distributions for the three catalysts are fairly similar. In addition, the formation of the Pt-Co bimetallic bond is detected in all catalysts according to EXAFS measurements (Tables 1, Table S2 and Figure S2). CO$_2$ hydrogenation was evaluated in a flow reactor at 300 °C, with the activity being presented using both conversion and turnover frequency (TOF) by normalizing with the CO uptake value from each catalyst. . One can see in Table 1 that the conversion of CO$_2$ over the three catalysts is very close, indicating that the selectivity can be significantly varied while maintaining similar conversion. The ratio of CO/CH$_4$ over PtCo/TiO$_2$ catalyst is 85, far higher than that over PtCo/CeO$_2$ (12) and PtCo/ZrO$_2$ (8.5), revealing that PtCo/TiO$_2$ selectively produces CO, while the other two supports favor the production of CH$_4$.

A batch reactor equipped with an FTIR spectrometer was used to monitor surface intermediates and gas-phase composition during the reaction. The FTIR spectra after the reaction of CO$_2$ and hydrogen on the PtCo/CeO$_2$ and PtCo/TiO$_2$ powder catalysts (Figure S3) are consistent with the findings from the AP-XPS study on the model surfaces (Figure 1). The 1373 cm^{-1} and 1610 cm^{-1} modes are assigned to the symmetric and antisymmetric OCO vibrations (Table S3), respectively, of formate-like species, suggesting the existence of HCOO*/HOCO* surface intermediates over both catalysts. In addition, on PtCo/CeO$_2$ vibrational features (peaks at 1420 cm^{-1} and 2869 cm^{-1}) indicative of the δ(CH$_3$) and v$_s$(CH$_3$) mode (Table S3) in *CH$_3$O[14] also appeared, revealing the presence of the *CH$_3$O intermediate.

The FTIR spectra of some of the characteristic vibrational modes were also employed to identify the gas-phase reaction products. The vibrational modes v(C=O) at 2358 cm^{-1}, v(C≡O) at 2170 cm^{-1} and v(C-H) at 3016 cm^{-1} were used to monitor the presence of CO$_2$, CO and CH$_4$, respectively. On PtCo/TiO$_2$, besides the sharp CO$_2$ peak, CO is also detected as a product (Figure 2a). On PtCo/CeO$_2$, vibrational peaks indicative of the formation of CH$_4$ are also observed in addition to CO.

The verification of surface reaction intermediates was also carried out by reacting CH$_3$OH and formic acid (HCOOH) into the batch reactor at the same conditions as CO$_2$ hydrogenation to monitor and compare the reaction products. As shown in Figure 2b, the reaction products are almost identical on both PtCo/CeO$_2$ and PtCo/TiO$_2$ catalysts. CO and CO$_2$ were produced from both CH$_3$OH and HCOOH, indicating that *HCOO is the likely reaction intermediate on both PtCo/CeO$_2$ and PtCo/TiO$_2$ catalysts. CH$_4$ is produced only from CH$_3$OH,

suggesting that the surface *CH$_3$O intermediate is the likely precursor for the formation of CH$_4$. However, the conversion of CH$_3$OH to CH$_4$ occurs on both surfaces. Accordingly, the role that the TiO$_2$ support in preventing the formation of *CH$_3$O and therefore CH$_4$ on PtCo/TiO$_2$ must relate to the steps before *CH$_3$O formation.

Overall, the experimental results on CeO$_2$ and TiO$_2$ supported PtCo powder catalysts indicate that different reaction intermediates lead to the difference in the CO/CH$_4$ selectivity in the flow reactor. The CO/CH$_4$ selectivity on PtCo/TiO$_2$ is much higher than that on PtCo/CeO$_2$ (Table 1). On PtCo/TiO$_2$, *HCOO is formed as the intermediate, which may eventually produce CO. On PtCo/CeO$_2$, besides the route via *HCOO, a pathway via *CH$_3$O intermediate runs in parallel, which likely leads to the formation of CH$_4$. Yet, at this stage the origin of oxide supports in tuning the selectivity is still unclear. It requires better understanding of the detailed reaction network and the active sites, which is extremely difficult to obtain merely using the experimental techniques. Therefore, DFT calculations were performed to determine the mechanisms for CO$_2$ hydrogenation at the metal-oxide interfaces.
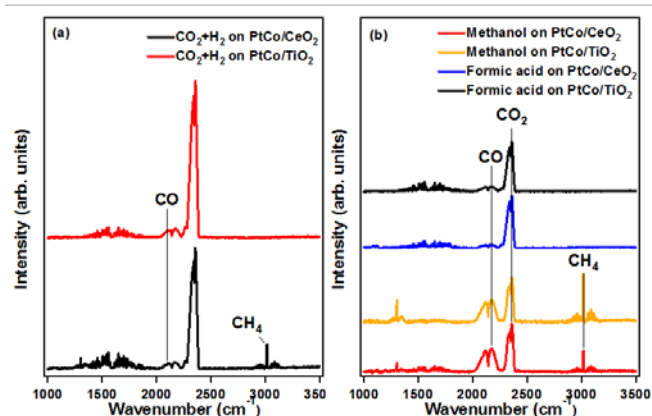

Figure 2. FTIR spectra during the reaction of (a) CO$_2$ reduction by H$_2$ and (b) formic acid and methanol on PtCo/CeO$_2$ and PtCo/TiO$_2$ catalysts.

The Pt-terminated surface structure has been predicted by DFT as the thermodynamically stable structure and detected in surface science experiments over model Co/Pt(111) surfaces[15] and Co/Pt thin films[16] for clean surfaces and in the presence of hydrogen. Figure S4 shows the DRIFTS measurements of CO adsorption over supported PtCo/ZrO$_2$. The relatively intense vibrational peaks of linearly-adsorbed CO of the bimetallic PtCo/ZrO$_2$ catalyst are much more similar to those of Pt/ZrO$_2$ than those of Co/ZrO$_2$, consistent with a Pt-terminated bimetallic surface. The PtCo-oxide interface was modeled by depositing a small oxide cluster on the PtCo(111) support, where a Pt$_{1ML}$/Co$_{1ML}$/Pt(111) near-surface model was used and the hydroxylation of oxides under hydrogen-rich environment was also considered (Figure 3). Such inverse model has been previously shown as a reasonable model to describe the catalytic properties of metal/oxide catalysts under CO$_2$ hydrogenation conditions.[3d, 8a, 17] Due to the deficiency of standard DFT in describing CeO$_x$, as discussed in more detail in SI,[18] PtCo/TiO$_2$ and PtCo/ZrO$_2$ were used in the current theoretical study as the representative catalysts selective to CO and CH$_4$, respectively.

The reaction network for CO$_2$ hydrogenation typically includes the reverse-water-gas-shift followed by CO hydrogenation (RWGS + CO-Hydro) pathways (Figure S5) and formate pathways.[19] Our results show that the binding

geometries of the reaction intermediates are similar on both PtCo/TiO$_2$ and PtCo/ZrO$_2$ (Figures S6 and S7). In general, C-bound species prefer Pt sites via a η^1-C$_{Pt}$ bonding, while O-bound species prefer the reduced M$^{\delta+}$ cation sites in metal oxides via a η^1-O$_M{}^{\delta+}$ configuration. In the case of species bound through both C and O (C,O-bound species, e.g. *CO$_2$, *HOCO, *CO, *CHO, *CHOH, *CH$_2$O and *CH$_2$OH), the metal-oxide interfacial sites are favored via a η^2-C$_{Pt}$O$_M{}^{\delta+}$ configuration. Thus the metal-oxide interface is likely to play an important role in activating chemically inert CO$_2$ and further facilitating its subsequent conversion.[3d, 8a]

CO and CH$_4$ production on PtCo/TiO$_2$ prefers undergoing the RWGS + CO-Hydro pathways, as shown in Figure 4a. The adsorption of CO$_2$ leads to the formation of carboxylate (CO$_2{}^{\delta+}$) due to the strong binding at the PtCo-TiO$_2$ interface, where the O-C-O bond is bent in an η^2-C$_{Pt}$O$_{Ti}{}^{\delta+}$ configuration (Figure S5b). Such binding motif favors the hydrogenation to *HOCO (Figure S5c) with a reaction energy (ΔE) of -0.56 eV and a small activation energy (E$_a$) of 0.23 eV, where the transition only involves one O-H bond formation with a small distortion in the geometry of *CO$_2$; in contrast, *CO$_2$ hydrogenation to *HCOO is kinetically and thermodynamically less favorable (ΔE = -0.25 eV, E$_a$ = 0.51 eV). The produced *HOCO then dissociates and forms *CO and *OH (ΔE= -0.26 eV, E$_a$= 0.93 eV), where *OH is hydrogenated to form *H$_2$O (E$_a$= 0.43 eV), while *CO either desorbs or undergoes further hydrogenation reactions. It is found that *CO hydrogenation to *CHO is exothermic by only -0.05 eV. The corresponding E$_a$ (1.40 eV) is comparable to BE of CO (-1.51 eV, Table S4). However, under the reaction conditions, the entropy contribution significantly lowers the barrier for *CO desorption by 1.28 eV at 300 °C, and the desorption barrier is much lower than that for the hydrogenation to *CHO. Thus, corroborating our experimental finding (Table 1), the DFT results show that CO(g) is the main product from CO$_2$ hydrogenation on PtCo/TiO$_2$.
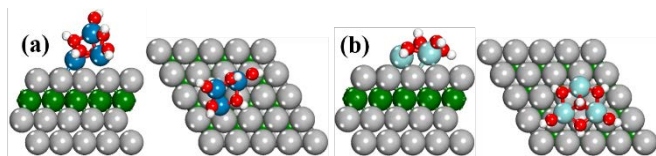

Figure 3. Side and top views of DFT-optimized structures for model hydroxylated Ti$_3$O$_6$/PtCo(111) (a) and Zr$_3$O$_6$/PtCo(111) (b) surfaces. Pt: light grey, Co: green, Zr: light blue, Ti: dark blue, H: white.

The minor products come from the formed *CHO, which can be hydrogenated to either *CH$_2$O or *CHOH. Figure 4a shows that the two steps are competitive with the difference in E$_a$ of only 0.06 eV (0.82 eV vs. 0.88 eV). *CHOH is the precursor for C-O bond cleavage to form *CH + *OH (ΔE= -0.42 eV, E$_a$ = 0.47 eV). *CH then undergoes three exothermic hydrogenation reactions to form CH$_4$, where the highest barrier is observed for *H + *CH$_3$ → *CH$_4$ + * (E$_a$= 0.48 eV). The produced *CH$_2$O is further hydrogenated to produce *CH$_2$OH (E$_a$= 0.49 eV), which dissociates to *CH$_2$ and *OH (ΔE= 0.10 eV and E$_a$= 0.86 eV) and leads to the production of *CH$_4$ eventually. In comparison the formation of *CH$_3$O (E$_a$= 0.60 eV) is less favorable. The DFT results agree well with the experiments on PtCo/TiO$_2$ model and powder catalysts, where *CH$_3$O intermediate and therefore CH$_3$OH(g) is not observed during the CO$_2$ hydrogenation. Therefore, the minor product for CO$_2$ hydrogenation on PtCo/TiO$_2$ is CH$_4$(g), consistent with the experimental results (Table 1).

In comparison, PtCo/ZrO$_2$ selectively strengthens the bindings of the C,O-bound and O-bound species at the interface

via O-Zr$^{\delta+}$ bonds (Table S4 and Figure S7), while for the C-bound species, the BE via Pt-C interaction is the same as that on TiO$_2$/PtCo(111). According to the calculated partial density of states (PDOS, Figure S8), the promoted O-Zr$^{\delta}$ interaction is associated with more electronic d-states near the Fermi level than that of Ti$^{\delta+}$. Thus, although the CO$_2$ hydrogenation follows the same pathways in both cases, differences in reaction and activation energies are clearly observed (Figure 4b). Compared to PtCo/TiO$_2$, *CO$_2$ hydrogenation to *HOCO (ΔE = -0.39 eV, E$_a$ = 0.11 eV), *HOCO dissociation to *CO and *OH (ΔE= -0.75 eV, E$_a$= 0.70 eV), as well as *CO hydrogenation to *CHO (ΔE= -0.48 eV, E$_a$= 0.98 eV) are more energetically favorable; in contrast *CO desorption is more difficult due to the stronger CO BE (-2.00 eV). In this case, even including the entropy contribution, *CO hydrogenation is compatible with *CO desorption (Gibbs free energy = 0.72 eV at 573K). Therefore, CO is only the minor product from PtCo/ZrO$_2$ while the major product should come from *CO hydrogenation, such as CH$_4$ and or CH$_3$OH.
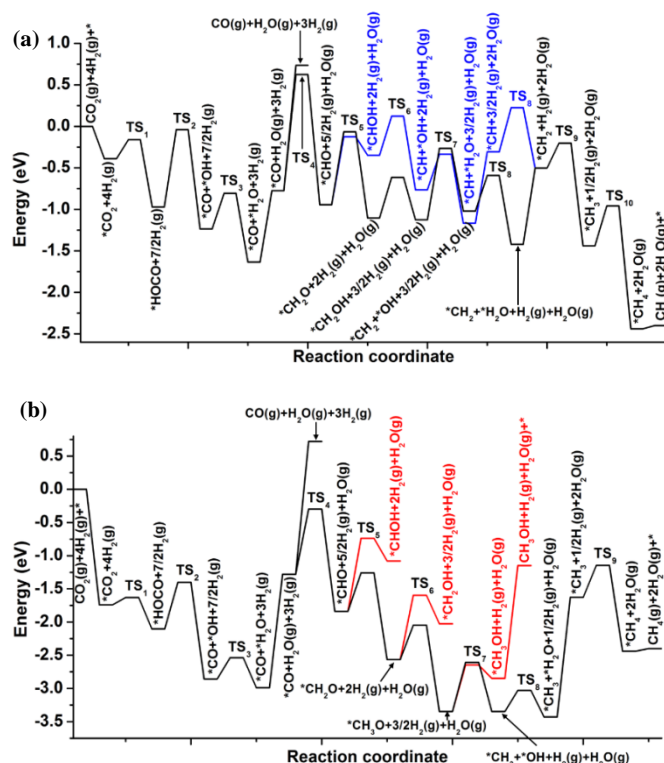

Figure 4. Potential energy diagrams for the CO, and CH$_4$ synthesis via the RWGS + CO-Hydro pathways on model hydroxylated Ti$_3$O$_6$/PtCo(111) (a) and Zr$_3$O$_6$/PtCo(111) (b) surfaces.

Furthermore, *CHO at the PtCo/ZrO$_2$ interface is preferentially hydrogenated to *CH$_2$O (ΔE= -0.74 eV, E$_a$= 0.58 eV), rather than *CHOH (ΔE= 0.76 eV, E$_a$= 1.10 eV) (Figure 4b). The sequential hydrogenation of *CH$_2$O results in *CH$_3$O formation (ΔE= -0.72 eV, E$_a$= 0.52 eV) in contrast to the endothermic formation of *CH$_2$OH (ΔE = 0.54 eV, E$_a$ = 0.97 eV). This is in good agreement with the experimental detection of the *CH$_3$O intermediate on the PtCo/ZrO$_2$ model surface (Figure 1) and powder catalyst (Figure S3). *CH$_3$O hydrogenation to *CH$_3$OH (ΔE= 0.50 eV, E$_a$= 0.70 eV) and to *CH$_3$ and *OH (ΔE = 0.01 eV, E$_a$ = 0.74 eV) are likely competitive; however, due to the favorable binding at PtCo-ZrO$_2$, desorption of *CH$_3$OH is highly uphill in energy by 1.72 eV. Furthermore, the formed *CH$_3$OH is not stable and prefers dissociation to *CH$_3$O (E$_a$=

0.20 eV) rather than desorption (E_a= 0.70 eV). In contrast, *CH$_3$ hydrogenation to form *CH$_4$ is much easier (ΔE= -0.95, E_a= 0.48 eV). Therefore, as observed experimentally (Table 1), the DFT calculations predict that CH$_4$ is the major product resulting from the hydrogenation of *CO on PtCo/ZrO$_2$. Finally, the most difficult step, likely activity-controlling step, along the reaction pathways (Figure 4) varies from *HOCO dissociation on PtCo/TiO$_2$ to *CO hydrogenation to *HCO on PtCo/ZrO$_2$; however, values of the corresponding barriers are similar (0.93 eV vs. 0.98 eV). Accordingly, a small decrease in TOF is expected, which agrees well with our measurement in Table 1.

In summary, our combined experiment-theory study shows that changing the oxide support from TiO$_2$ to CeO$_2$ or ZrO$_2$ provides the possibility to tune the selectivity of bimetallic PtCo catalysts for CO$_2$ hydrogenation; in contrast much smaller effect is observed for the overall activity. CeO$_2$ or ZrO$_2$ supported PtCo catalysts display high selectivity to CH$_4$, while CO is preferred by using the TiO$_2$ support. According to the AP-XPS for model surfaces and FTIR spectra for powder catalysts, the difference in selectivity is likely associated with the variation in dominant reaction pathways, where *HCOO/*HOCO is observed as the reaction intermediates on PtCo/TiO$_2$, while both *HCOO/*HOCO and *CH$_3$O are observed on PtCo/CeO$_2$ or PtCo/ZrO$_2$. The DFT study well describes the experimental observations and indicates that the metal-oxide interface promotes the heterogeneity of active sites and enables moving away from the linear scaling of adsorbate binding energies. The bindings of the C,O-bound and O-bound species are tuned selectively at the interface, rather than the C-bound species. The variation of support from TiO$_2$ to ZrO$_2$ does not affect the dominant RWGS + CO hydrogenation pathways; however, the CO production is hindered and the CO hydrogenation to CH$_4$ is turned on over ZrO$_2$. Our study highlights that the synergy between metal and oxide at the metal-oxide interface plays an important role in tuning the selectivity of CO$_2$ hydrogenation reaction on oxide supported PtCo bimetallic catalysts. More importantly, it confirms the possibility in fine-tuning the catalytic selectivity through the metal-oxide interfaces.

Experimental Section

The catalysts were prepared by the incipient wetness impregnation method with an aqueous solution of the respective metal precursors ((NH$_3$)$_4$Pt(NO$_3$)$_2$ and Co(NO$_3$)$_2$•6H$_2$O from Alfa Aesar). The metal loadings (wt%) of the PtCo bimetallic catalysts were 1.7% Pt and 1.5% Co. After impregnation, the samples were dried at 60 °C overnight and calcined in air at 290 °C for 2 hours. The PtCo bimetallic catalyst was selected because it showed better CO$_2$ conversion activity than the corresponding monometallic catalysts.[3e]

The DFT calculations were performed using the Vienna Ab-Initio Simulation Package (VASP) code.[20] Electron-ion interactions were treated by the projector augmented wave (PAW) method. The exchange and correlation energy was described using the generalized gradient approximation with the Perdew-Wang (PW91) functional. Cutoff energy of 400 eV and a 3 × 3 × 1 Monkhorst-Pack k points were used. Further details of the theoretical models and experimental synthesis/characterization are provided in the Supporting Information.
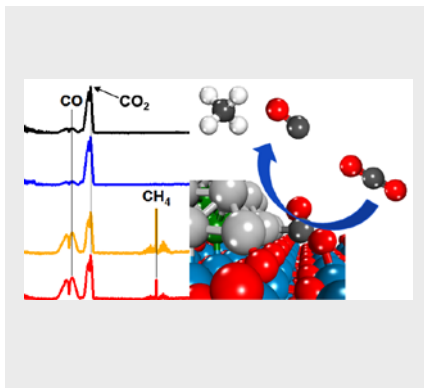
Acknowledgements

[1] P. Sabatier, *La catalyse en chimie organique*, Librairie Polytechnique, Paris et Liège **1920**.

[2] a) F. Calle-Vallejo, J. Tymoczko, V. Colic, Q. H. Vu, M. D. Pohl, K. Morgenstern, D. Loffreda, P. Sautet, W. Schuhmann, A. S. Bandarenka, *Science* **2015**, *350*, 185-189; b) J. K. Norskov, T. Bligaard, J. Rossmeisl, C. H. Christensen, *Nat. Chem.* **2009**, *1*, 37-46.

[3] a) D. J. Stacchiola, S. D. Senanayake, P. Liu, J. A. Rodriguez, *Chem. Rev.* **2013**, *113*, 4373-4390; b) E. A. Monyoncho, S. Ntais, N. Brazeau, J.-J. Wu, C.-L. Sun, E. A. Baranova, *ChemElectroChem* **2016,** *3*, 218-227; c) G. R. Jenness, J. R. Schmidt, *ACS Catal.* **2013**, *3*, 2881-2890; d) J. Graciani, K. Mudiyanselage, F. Xu, A. E. Baber, J. Evans, S. D. Senanayake, D. J. Stacchiola, P. Liu, J. Hrbek, J. F. Sanz, J. A. Rodriguez, *Science* **2014**, *345*, 546-550; e) M. D. Porosoff, J. G. G. Chen, *J. Catal.* **2013**, *301*, 30-37; f) Y. Hartadi, D. Widmann, R. J. Behm, *ChemSusChem* **2015**, *8*, 456-465.

[4] a) K. Mudiyanselage, S. D. Senanayake, L. Feria, S. Kundu, A. E. Baber, J. Graciani, A. B. Vidal, S. Agnoli, J. Evans, R. Chang, S. Axnanda, Z. Liu, J. F. Sanz, P. Liu, J. A. Rodriguez, D. J. Stacchiola, *Angew. Chem. Int. Ed.* **2013**, *52*, 5101-5105; b) A. Bruix, J. A. Rodriguez, P. J. Ramírez, S. D. Senanayake, J. Evans, J. B. Park, D. Stacchiola, P. Liu, J. Hrbek, F. Illas, *J. Am. Chem. Soc.* **2012**, *134*, 8968-8974; c) F. Calaza, C. Stiehler, Y. Fujimori, M. Sterrer, S. Beeg, M. Ruiz-Oses, N. Nilius, M. Heyde, T. Parviainen, K. Honkala, H. Häkkinen, H.-J. Freund, *Angew. Chem. Int. Ed.* **2015**, *54*, 12484-12487; d) J. Y. Park, L. R. Baker, G. A. Somorjai, *Chem. Rev.* **2015**, *115*, 2781-2817.

[5] J. Saavedra, H. A. Doan, C. J. Pursell, L. C. Grabow, B. D. Chandler, *Science* **2014**, *345*, 1599-1602.

[6] a) M. G. Willinger, W. Zhang, O. Bondarchuk, S. Shaikhutdinov, H.-J. Freund, R. Schlögl, *Angew. Chem. Int. Ed.* **2014**, *53*, 5998-6001; b) L. Yu, Y. Liu, F. Yang, J. Evans, J. A. Rodriguez, P. Liu, *J. Phys. Chem. C* **2015**, *119*, 16614-16622; c) J. C. Matsubu, V. N. Yang, P. Christopher, *J. Am. Chem. Soc.* **2015**, *137*, 3076-3084.

[7] a) M. A. A. Aziz, A. A. Jalil, S. Triwahyono, A. Ahmad, *Green Chem.* **2015**, *17*, 2647-2663; b) G. Melaet, W. T. Ralston, C.-S. Li, S. Alayoglu, K. An, N. Musselwhite, B. Kalkan, G. A. Somorjai, *J. Am. Chem. Soc.* **2014**, *136*, 2260-2263.

[8] a) X. F. Yang, S. Kattel, S. D. Senanayake, J. A. Boscoboinik, X. W. Nie, J. Graciani, J. A. Rodriguez, P. Liu, D. J. Stacchiola, J. G. G. Chen, *J. Am. Chem. Soc.* **2015**, *137*, 10104-10107; b) C. Liu, B. Yang, E. Tyo, S. Seifert, J. DeBartolo, B. von Issendorff, P. Zapol, S. Vajda, L. A. Curtiss, *J. Am. Chem. Soc.* **2015**, *137*, 8676-8679.

[9] a) M. D. Porosoff, X. F. Yang, J. A. Boscoboinik, J. G. Chen, *Angew. Chem. Int. Ed.* **2014**, *53*, 6705-6709; b) H.-K. Lim, H. Shin, W. A. Goddard, Y. J. Hwang, B. K. Min, H. Kim, *J. Am. Chem. Soc.* **2014**, *136*, 11355-11361; c) C. Costentin, S. Drouet, M. Robert, J.-M. Savéant, *Science* **2012**, *338*, 90-94.

[10] W.-H. Cheng, *Acc. Chem. Res.* **1999**, *32*, 685-691.

[11] a) L. C. Grabow, M. Mavrikakis, *Acs Catal.* **2011**, *1*, 365-384; b) Y. Yang, J. Evans, J. A. Rodriguez, M. G. White, P. Liu, *Phys. Chem. Chem. Phys.* **2010**, *12*, 9909-9917.

[12] a) W. L. Zhu, Y. J. Zhang, H. Y. Zhang, H. F. Lv, Q. Li, R. Michalsky, A. A. Peterson, S. H. Sun, *J. Am. Chem. Soc.* **2014**, *136*, 16132-16135; b) Q. Lu, J. Rosen, Y. Zhou, G. S. Hutchings, Y. C. Kimmel, J. G. G. Chen, F. Jiao, *Nat. Commun.* **2014**, *5,* 3242; c) S. Back, M. S. Yeom, Y. Jung, *Acs Catal.* **2015**, *5*, 5089-5096.

[13] X. Deng, A. Verdaguer, T. Herranz, C. Weis, H. Bluhm, M. Salmeron, *Langmuir* **2008**, *24*, 9474-9478.

[14] T. G. Kelly, A. L. Stottlemyer, H. Ren, J. G. Chen, *J. Phys. Chem. C* **2011**, *115*, 6644-6650.

[15] C.A. Menning, H.H. Hwu, J.G. Chen, *J. Phys. Chem. B* **2006**, 110, 15471-15477.

[16] C.A. Menning, J.G. Chen, *J. Power Sources* **2010**, 195, 3140-3144

[17] T. Lunkenbein, J. Schumann, M. Behrens, R. Schlögl, M. G. Willinger, *Angew. Chem. Int. Ed.* **2015**, *54*, 4544-4548.

[18] D. Lu, P. Liu, *J. Chem. Phys.* **2014**, *140*, 084101.

[19] P. Liu, Y. Yang, M. G. White, *Surf. Sci. Rep.* **2013**, *68*, 233-272.

[20] a) G. Kresse, J. Furthmuller, *Comp. Mater .Sci.* **1996**, *6*, 15-50; b) G. Kresse, J. Furthmuller, *Phys. Rev. B* **1996**, *54*, 11169-11186.

Entry for the Table of Contents (Please choose one layout)

COMMUNICATION

The selectivity of CO_2 hydrogenation reaction of Metal-Oxide catalysts can be tuned by varying oxide supports.

Shyam Kattel,[#] Weiting Yu,[#] Xiaofang Yang, Binhang Yan, Yanqiang Huang, Weiming Wan, Ping Liu*, Jingguang G. Chen*

Page No. – Page No.
CO_2 Hydrogenation on Oxide-supported PtCo Catalysts: Fine-tuning Selectivity using Oxide supports